1D scanning arrays on dense dielectrics using PCS-EBG technology

1-D Scanning Arrays on Dense Dielectrics Using PCS-EBG Technology

Nuria Llombart, *Member, IEEE*, Andrea Neto, *Member, IEEE*, Giampiero Gerini, *Member, IEEE*, and Peter de Maagt, *Senior Member, IEEE*

***Abstract*—We show how the design of integrated arrays can significantly benefit from planar circularly symmetric (PCS) electromagnetic band gap (EBG) structures. Using this technology, a phased array that scans up to 40° in one dimension and that is characterized by relatively large bandwidth (BW $\approx$ 15%) is designed, manufactured and tested. The specific advantages coming from the use of PCS-EBGs are two fold. On one hand the losses associated to surface waves are significantly reduced. On the other hand each element of the array has a larger effective area that leads to a higher gain for the complete array when compared with a standard technology. Additional benefits are the low cross-polarization levels, the good front to back ratio considering that the antenna does not include a backing reflector, and the low profile.**

***Index Terms*—Electromagnetic band gap (EBG) , phased arrays, printed technology, surface waves.**

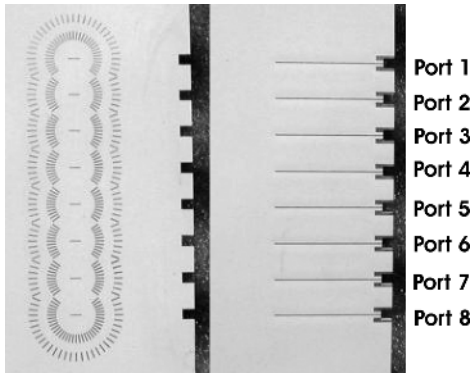

Fig. 1. 1-D scanning array composed of 8 elements with PCS-EBGs (front and back view).

I. Introduction

SYNTHETIC aperture radar (SAR) [1], [2] is a field where there is a demonstrated need for low profile phased array antennas. Typical requirements for SAR applications involve bandwidths (BW) larger than 10% and scanning angles up to 40 degrees in the longitudinal plane.

Although a SAR system is selected to set the requirements, the main objective of this work is to present a strategy to develop innovative antenna architectures, based on EBG technology, which can meet fundamental requirements for integrated front-ends like: low cost, low profile, high gain and ease of integration with the transmit/receive (T/R) modules. The radiating elements are resonant dipoles printed on the opposite side of a metallic plane that constitutes the ground for the microstrip feeding lines and the T/R modules. The electromagnetic coupling between the two half spaces defined by the ground plane is achieved via resonant slots. There are two significant advantages in using both planar antennas and T/R modules. The first advantage is that it is inexpensive since the number of manufacturing steps are reduced with respect to other technologies that require cavity backing or vertical metallic connections to transfer the signal vertically from the lower feeding planes to the antennas. The second one is that spurious radiation from the vertical connections can affect the level of cross polarization as explained in [2] and [3].

When SAR systems are placed in airplanes, the available power budget is very limited, and differences as low as 1 dB in the gain can lead to the preference of one technology with respect to others. Focusing the attention on planar structures and aiming at large efficiencies, an issue that arises at early stage is the optimization of the front to back ratio. A convenient approach to address this issue is based on the use of dense (high permittivity) dielectric slabs. This allows maximizing the front radiation in comparison to the power radiated on the back side of the structure. Alternative solutions, using non dense dielectrics in the radiating half spaces, necessitate the introduction of a backing reflector in order to control the backscattering of the antenna. By doing this, these structures then face a problem of parallel plate waveguide modes. Therefore, this solution potentially shifts the design difficulties from the antenna layer to the feeding layer. The adoption of dense dielectric antenna substrates offers the advantage of simplifying the overall structure, because avoiding the use of a backing reflector offers an easily accessible interface for the connection of the antenna and the T/R modules. As a drawback, thick dielectric layers of high permittivity support surface wave propagation, whose control now becomes the key design issue.

The advantages associated to the planarity of the structures can be achieved, without loss of performances using planar circularly symmetric electromagnetic band gap substrates (PCS-EBG). An example of such planar array with PCS-EBG is shown in Fig. 1.

Most of the pioneering work on the use of EBG for phased arrays typically focused on the reduction of the scan blindness

Manuscript received February 9, 2006; revised August 6, 2006. This work was supported by ESTEC under contract 17539/03/NL/JA from the European Space Agency.

N. Llombart, A. Neto, and G. Gerini are with TNO Defence, Security and Safety, Den Haag 2597 AK, The Netherlands (e-mail: nuria.llombartjuan, andrea.neto, giampiero.gerini@tno.nl).

P. de Maagt is with the Electromagnetics Division, European Space Agency, 2200 AG, Noordwijk, The Netherlands (e-mail: Peter.de.Maagt@esa.int).

Color versions of one or more of the figures in this paper are available online at http://ieeexplore.ieee.org.

Digital Object Identifier 10.1109/TAP.2006.888435

problem and the possibility to reduce mutual coupling between adjacent elements, [4], [5]. In a recent work from Iluz *et al.* [6], EBG structures were adopted in a phased arrays demonstrator, interleaving EBG and antenna rows, with the objective of reducing the mutual coupling between the array elements. This demonstrator was designed, manufactured and tested showing an actual reduction of the coupling between elements of different rows, in the plane perpendicular to the EBG structure. As a side effect, an increased coupling between elements of the same row was observed. Measurements demonstrated an operational bandwidth of the array antenna in the order of 2.5%.

On the contrary, this work aims at reducing the surface wave launched by the array elements in order to increase the gain and avoid the effects of its diffraction at the edges of the substrate.

The issue of the bandwidth achievable is one aspect to which this paper devotes particular attention with a focus on 1-D (or predominantly 1-D) scanning arrays. The feasibility of an EBG based array with BW up to 15% has actually been demonstrated with the design, manufacturing and testing of hardware breadboards.

The paper is structured as follows. In Section II, the reasons why PCS-EBGs are suitable for use in 1-D scanning arrays are clarified and the array demonstrator is introduced. In Section III the measured and simulated S-parameters are compared and the reasons why the configuration of the demonstrator does not induce scan blindness are clarified. In Section IV the beam forming network and the effect of the coherent excitation of the different elements of the array are discussed. In particular the role of the global surface wave excited on the array substrate is clarified in the presence and in absence of the EBGs. The measured active reflection coefficients are then described. In Section V the measured radiation patterns are discussed.

Throughout the paper, qualitative physical insight as well quantitative numerical simulations clarify the overall wave phenomena involved with the beam scanning.

II. Design of Arrays Based on PCS-EBGs

The array element considered in this section is shown in Fig. 2. It consists of two dielectric slabs with the same dielectric constant ϵ_r and different heights h and h_m divided by a ground plane. The slot etched in the ground plane is coupled to an orthogonal dipole located on the top of the upper dielectric slab h. Finally, the structure is excited via a microstrip printed on the other side of the lower dielectric slab h_m. The antenna is surrounded by a PCS-EBG consisting on two rings of radial dipoles.

The analysis and design of single antennas surrounded by a PCS-EBG structure have been the subject of two previous papers, [7], [8]. In [7], the PCS-EBG concept was introduced together with the design of the length of the dipoles l_g and the radial period d in order to obtain a band gap in the bandwidth of interest. Moreover, a single slot coupled dipole surrounded by a PCS-EBG was manufactured and measured, showing excellent performances in terms of bandwidth and efficiency. In [8], a detailed explanation of the wave phenomenon that leads to the best possible theoretical performances in terms of bandwidth for single PCS-EBG antennas was given. In order to simplify the analysis without significant loss of generality, a slot antenna

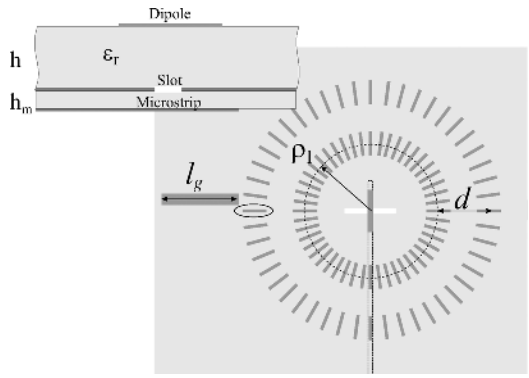

Fig. 2. Array element: slot coupled to a dipole, excited via microstrip and surrounded by a PCS-EBG.

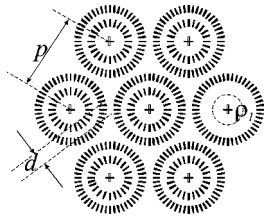

Fig. 3. Array of antennas each one surrounded by PCS-EBG.

was studied. A simplified quasi analytical model for the characterization of the interaction between the central antenna and the surrounding EBG was also presented and discussed. As design guideline, the optimal radiation bandwidth (defined as the range of frequency over the antenna radiates with high efficiency) for printed antennas on grounded dense dielectric slabs ($\epsilon_r \approx 10$) and surrounded by EBGs was achieved when:

1) the height of the dielectric slab at the central frequency is in the order of $0.18\lambda_d$ with λ_d the wavelength in the dielectric ($\lambda_d = \lambda_0/\sqrt{\epsilon_r}$)
2) the equivalent cavity defined by the PCS-EBG has a radius (ρ_1 in Fig. 3) approximately equal to half of the TM_0 surface wave wavelength (λ_{TM0}):

$$\rho_1 \approx \frac{\lambda_{TM0}}{2}. \tag{1}$$

Even though these conclusions were demonstrated for slot antennas only, they can be extended to other central resonant antennas. Moreover the radius dimensioning (distance between the antenna and the EBG) applies also to EBG structures realized with technologies that are not planer (e.g., based on metal vias).

An array composed of elementary cells that host a central resonant antenna surrounded by a circular symmetric EBG (see Fig. 3) would be an optimal structure to homogenize the surface wave attenuation in all directions. However, a preliminary design exercise already rules out such arrays for applications that need electronic beam scanning capabilities over a wide bandwidth. The qualitative motivation is based on two basic design rules: on one side, the dimensioning of the EBG structure of each unit cell in order to optimize the frequency BW of the array

element in presence of the EBG; and, on the other side, the dimensioning of the inter-element distance (array lattice) based on the required scanning performances of the array.

To achieve wide BW, the radius of each equivalent EBG cavity ρ_1 must be as in (1). Moreover, the distance (d) between the rings composing the EBG structure of each unitary cell is dictated by the required frequency band gap [7]. Therefore, it is evident that the overall dimension of the array unit cell is fixed by the BW requirements, depends on the permittivity of the dielectric substrate and might be in conflict with the required inter-element distance even for relatively small scanning angles.

In conclusion, it turns out that in order to fit an elementary cell (antenna and EBG rings) in an array lattice that allows 2-D scanning over wide angular region (e.g., $\pm 60°$) without grating lobes, the only available parameter to reduce the EBG dimensions is the dielectric constant of the antenna substrate. However, the dielectric constant that would be necessary is believed to be too large, $\epsilon_r > 30$, for such arrays to be manufacture at reasonable cost at the present time.

A. Array Demonstrator

The PCS-EBG concept is well suited for 1-D scanning arrays. The main design principle is to use linearly polarized antenna elements arrayed in the H-plane. In [7] was demonstrated that a slot coupled dipole launches TM surface waves predominantly in the E-plane cut of the slab with a $cos\phi$ angular distribution of the field intensity [Fig. 4(a)]. Fig. 4(b) shows the total electric field inside the substrate launched by an aperture coupled dipole simulated by means of the commercial software MWS from CST [10], where one can clearly see the dominant TM waves as in Fig. 4(a). For this reason, one could use PCS-EBGs to reduce the TM waves only in a specific angular sector, where the waves are predominantly launched. In the example shown in Fig. 4(c), $\phi \in [-38°, 38°] \cup [-142°, 142°]$ is the angular sector where the surface propagation is blocked. Integrating the $cos^2\phi$ power distribution over this sector, one obtains that 73% of the surface wave power is blocked. The angular sector concept allows closer spacing of the array elements, with respect to the cases when full rings were employed, leading to better scanning performance in the H-plane.

An *X*-band demonstrator composed of eight slot coupled dipoles arrayed in the H plane (Fig. 1) was designed and manufactured. The array is printed on dielectric material with $\epsilon_r = 9.8 \pm 0.245$ commercially available from Rogers. The design of the EBG is performed as explained in [7] and [8]. The parameters defining the EBG are the same than the ones in [7] but scaled to operate at *X*-band (10–12 GHz): $\rho_1 = 9$ mm, $d = 6.85$ mm, $l_g = 3.3$ mm. The main difference is that the PCS-EBG is only present in an angular sector region α. All antennas are fed via 50 Ω microstrip lines of the same length connected to coaxial cables. In order to have a maximum scanning without grating lobes of 51.8° at 12 GHz, the array period is fixed to 14 mm. Once the dimension of the periodic cell and of the inner radius ρ_1 is fixed, the angle α is also essentially fixed, which in the present case corresponds to $\alpha = 38°$.

III. S Parameters of Embedded Elements

First, the S parameters of the embedded elements (single element being fed and the rest of the elements matched with a load) were measured using an HP 8510 network analyzer. A time gating procedure was used to extract the effects of the small mismatch introduced by the microstrip-to-coax connectors (sub-miniature push-on (SMP) adaptors). Fig. 5 shows the measured and simulated reflection coefficients S_{ii} of all the ports (see Fig. 1). Symmetrical ports are presented in the same graphs to give an idea of the accuracy and repeatability of the measurements. For comparison reasons, the S_{11} parameter of the same array without PCS-EBG is also reported in Fig. 5(a). Fig. 6 shows the measured and simulated S_{12}, S_{13}, S_{14} and S_{15}, together with the correspondent S parameters of the same array without PCS-EBG. The agreement between measurements and calculations is good besides a frequency shift that has been systematically observed in all the measured S-parameters. Such frequency shift is coherent with the tolerance in the dielectric constant. The agreement validates the use of the MoM based commercial tool Ansoft Designer [9] to analyze the impedance properties of these structures. For all the PCS-EBG array elements the S_{ii} parameters were lower than -10 dB over a relatively large BW (in the order of 20%). This bandwidth is larger than the case without EBGs thanks to the cavity effect created by the PCS-EBG as explained in [8]. These encouraging initial results still need to be confirmed by the measurements of the active reflection coefficients and radiation patterns of the array, under different scanning conditions. These measurements, which were performed connecting the array to a simple beam-former, will be discussed in the next sections.

There is one more aspect, which needs some further considerations. The mutual coupling between adjacent antennas, for example S_{12} in Fig. 6, is slightly higher (-17 dB) than the value simulated in absence of the EBG ring sectors (-21 dB). Moreover, the S_{13}, S_{14} and S_{15} are also larger than in case of no

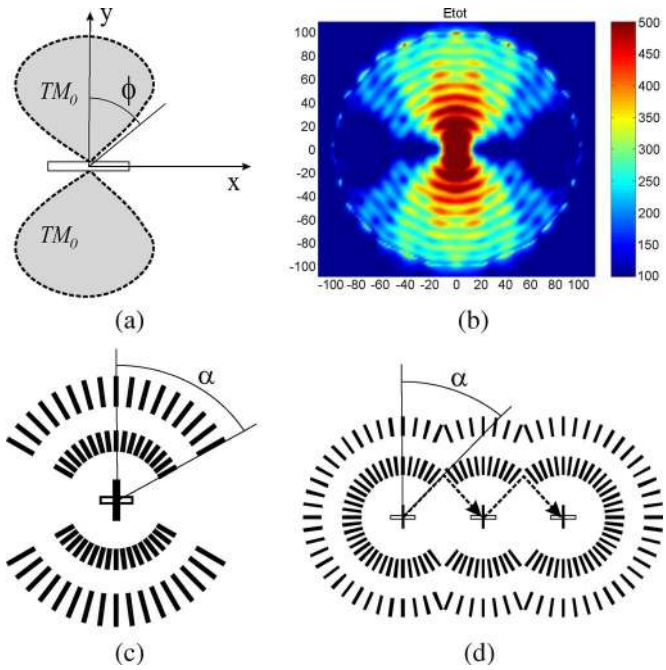

Fig. 4. (a) ϕ distribution of the TM electric field radiated by the antenna. (b) 2-D cut of the total electric field inside the substrate launched by an aperture coupled dipole (MWS CST simulation). (c) Reduced EBG configuration that allows to control 73% of the power. (d) Residual surface wave mechanism.

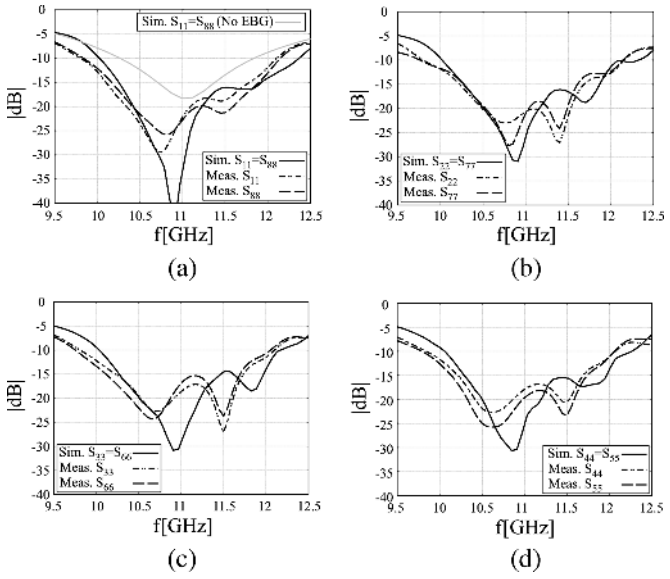

Fig. 5. Measured and calculated input S-parameters for the 1-D array prototype: (a) S_{11} and S_{88}, (b) S_{22} and S_{77}, (c) S_{33} and S_{66}, and (d) S_{44} and S_{55}. Figure (a) also includes the simulated S_{11} parameter of the same array without PCS-EBG

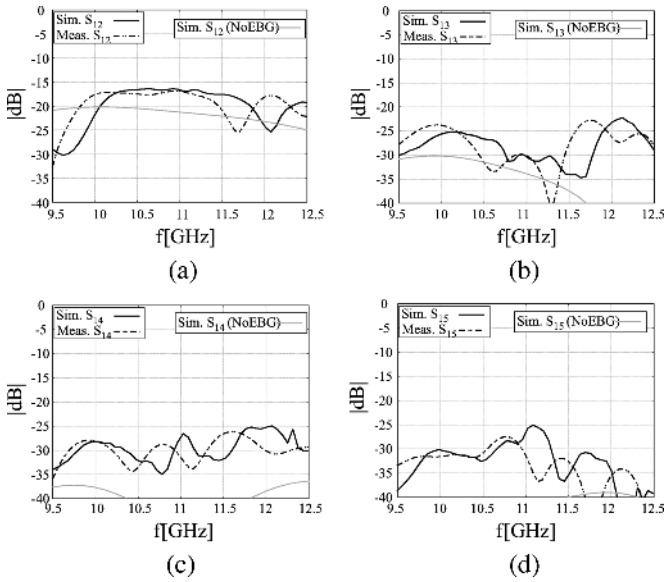

Fig. 6. Measured and simulated coupling parameters for the 1-D array prototype: (a) S_{12}, (b) S_{13}, (c) S_{14} and (d) S_{15}. In all the figures the correspondent S parameters of the same array without PCS-EBG are also reported.

EBGs. The reason why the inclusion of the EBGs increases the mutual coupling can be explained as follows: in addition to the power that couples directly to the adjacent element (absence of EBGs), also another small portion of power is coupled from the first antenna to the second one, via surface waves that in this case are reflected by the ring's edges [see Fig. 4(d)]. The increase of mutual coupling will not disturb the array performances in terms of scan blindness as explained in next section.

A. Scan Blindness in 1-D Arrays

For the present case, the relevant Floquet waves (FWs) have $k_{xm} = k_0 \sin\theta + (2\pi m/d_x)$. In Fig. 7, the spectral plane k_x, k_y is drawn. Let us define $k_\rho = \sqrt{k_x^2 + k_y^2}$. The two circles pertinent to $k_\rho = k_{\rm sw}$, where $k_{\rm sw}$ is the propagation constant of the dominant TM_0 wave, and to $k_\rho = k_0$, with k_0 the free space propagation constant, are both plotted. On the k_x axis, the FWs of lower indices ($m_x = -1$, $m_x = 0$, $m_x = 1$) are drawn with continuous circles for broad side beams. Dashed circles instead represent the location of the corresponding FW when the beam is scanning to the maximum pointing angle, $\theta_{\max}$. All the FWs move, maintaining the distances between them, as the array beam is scanned (this movement is represented by the arrows in Fig. 7). With this movement the circle of radius $k_{\rm sw}$ is crossed by the $m_x = -1$ FW, which would imply scan blindness if the slots were not presenting a null of surface wave radiation along $\mathbf{i}_x$

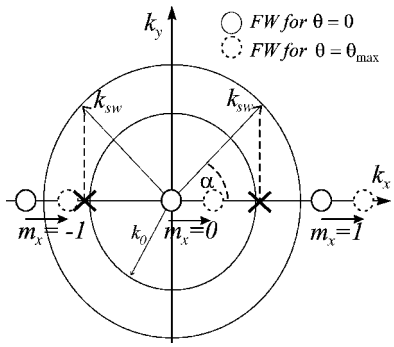

Fig. 7. Spectral plane and FW displacement as a function of the scanning angle.

With the EBG configuration of Fig. 4, there is some coupling via surface waves between two adjacent elements, but such coupling does not disturb significantly the array performances. In fact, this level of coupling cannot induce scan blindness problems in the present demonstrator. The only surface wave contributing to the mutual coupling between different slots in the array are those reflected at the intersection between two EBG rings. Let us assume that α is the angle that the direct and reflected waves at the ring edges form with the y-axis, see Fig. 4(d). The corresponding projection into the k_x axis is $k_{\rm sw} \sin\alpha$. Since this projection is necessarily smaller than $k_{\rm sw}$, the beam radiation angle at which scan blindness could occur, i.e., when the FW of index -1 would intercept the $k_\rho = k_{\rm sw} \sin\alpha$ circle, is greatly enlarged with respect to $k_{\rm sw}$. The location of this scanning direction is represented in the k_x, k_y by the crosses on the k_x axis. In the present case, $\alpha = 38°$ and $k_{\rm sw} = 1.49k_0$ at 12 GHz , then the scan blindness effect occurs for $\theta = 60.3°$, outside the free grating lobes scanning region, 51.8°.

IV. Active Array

After having measured the S-parameters, the array was fed by means of a beam former. The beam former uses Wilkinson power dividers and manually adjustable phase shifters to obtain uniform amplitudes and linearly tapered phases in the array. The beam forming network is shown in Fig. 8(a).

A. Surface Wave Considerations

The simultaneous excitation of all the elements has a considerable effect on the matching and radiation properties of the array under operational situations. On one side the coherent

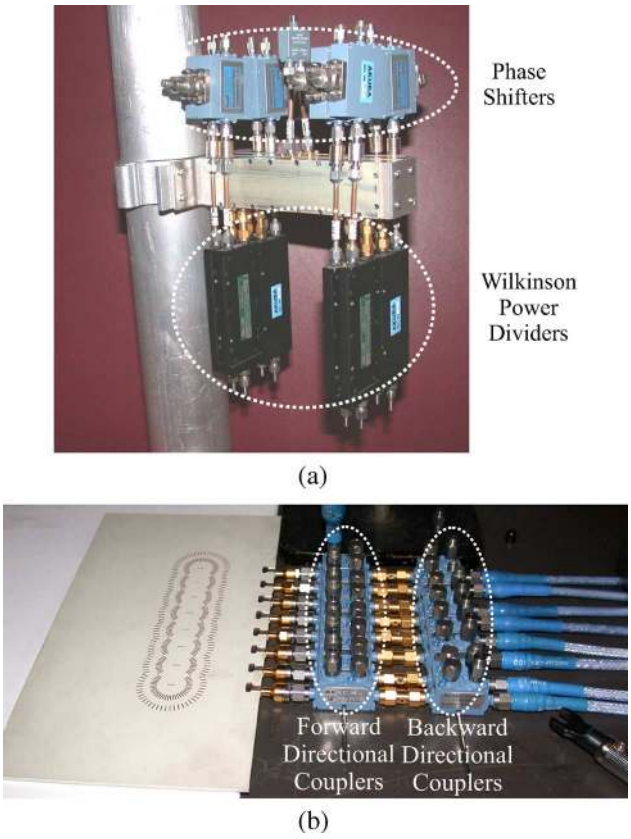

Fig. 8. (a) View of the beam former composed of Wilkinson power dividers and adjustable phase shifters. (b) View of the array fed by the directional couplers (one for each signal direction) placed before the coaxial to microstrip connections.

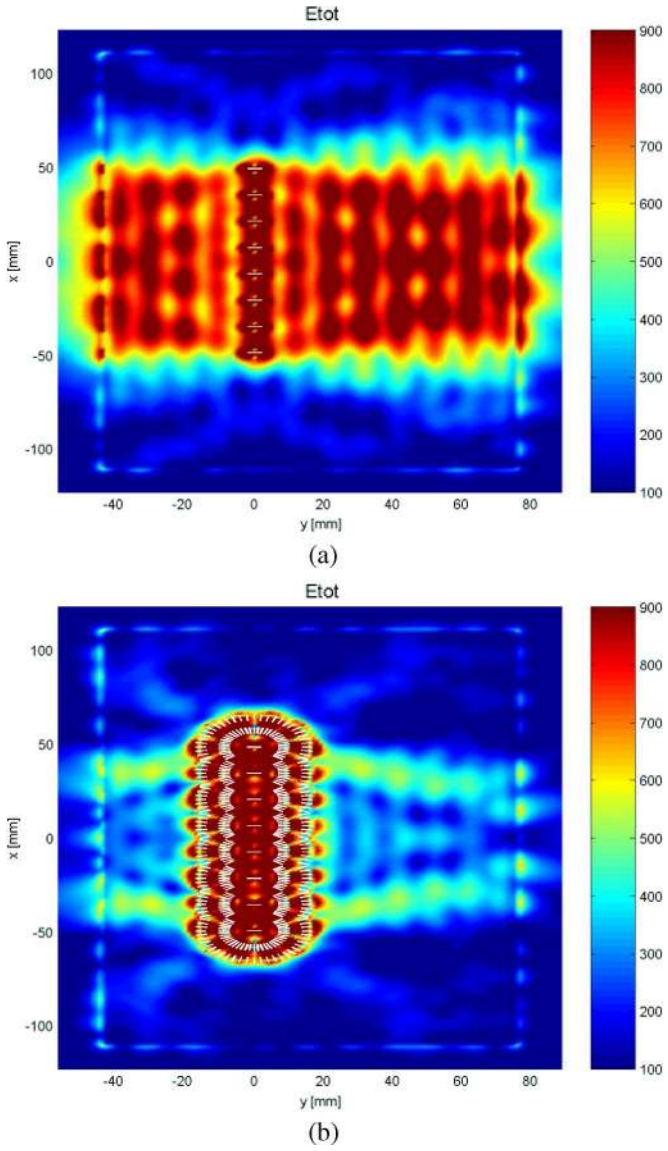

Fig. 9. 2-D cut of the total electric field inside the slab for $z = 1\,\mathrm{mm}$ with (a) no EBGs and (b) with EBGs. The dimensions of the slab are 120 mm × 220 mm.

radiation from all the elements generates the wanted radiated beam in free space, $k_{x0} = k_0 \sin\theta$. On the other side, the coherent excitation of surface waves by each array element generates a global surface wave propagation along the substrate, $k_{x0} = k_{\mathrm{sw}} \sin\theta_{\mathrm{sw}}$. To visualize such a global surface wave, two equivalent finite arrays, with and without the EBGs, were simulated by CST for broadside radiation. The phase fronts of the global surface wave on the substrate can be clearly observed in Fig. 9(a) for the case without EBGs. For the case with EBGs, Fig. 9(b), the shape of the surface wave fields generated by the array is qualitatively the same but the amplitude is significantly smaller. In both of the figures, the array structure has been indicated with white lines. In Fig. 10, the amplitudes of the z oriented electric field for the configurations with and without EBGs are compared in detail. The fields are observed at $z = 1\,\mathrm{mm}$ inside the substrate, in a cut orthogonal to the array direction that includes the center of the array. Note that two of the edges of the finite size dielectric slab are at different distance from the array center. It is evident that the EBG confines most of the fields in the *cavity* region. Outside the cavity the fields associated to the EBG case are about three times smaller than the ones associated to the case without EBGs. Using the results of these full wave simulations one can estimate the surface efficiency of the arrays. In this case, we define the surface wave suppression efficiency as the ratio between the sum of the power radiated by the antennas, P_a, and the power radiated by the EBGs, P_{EBG}, when present, and the total power given to the input ports P_{in} (which includes the one associated to the diffraction occurring at the edges of the truncated slab):

$$\eta_{\mathrm{sw}} = \frac{P_a + P_{\mathrm{EBG}}}{P_{\mathrm{in}}}. \tag{2}$$

These efficiencies are $\eta_{\mathrm{sw}}^{\mathrm{no-EBG}} \approx 41\%$ and $\eta_{\mathrm{sw}}^{\mathrm{EBG}} \approx 85\%$ when the array is operated with and without the EBGs, respectively.

Such efficiency values are in line with the ones that were obtained for a single antenna surrounded by PCS-EBG in [7]. In that case, the conclusion was simply that contributions arising from diffraction of surface waves at the end of the dielectric slabs could be neglected, because they were considerably smaller than the contributions associated to the antenna itself. This was confirmed by the comparison of the measured radiation patterns with the ones predicted by numerical tools that

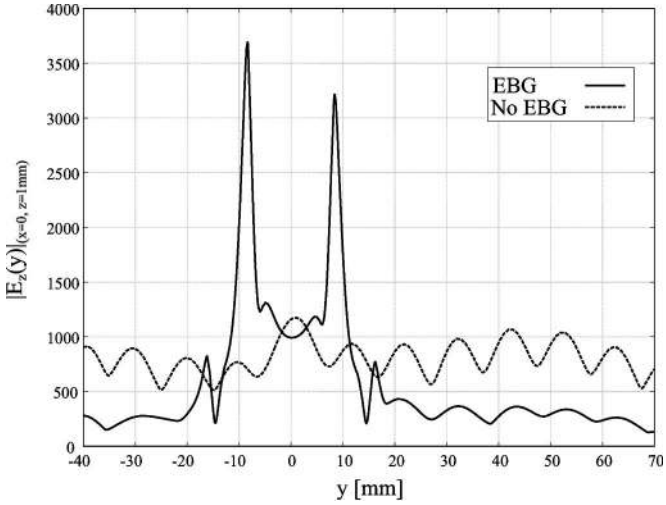

Fig. 10. Z component of the electric field inside the slab for $x = 0$ and $z = 1\,\mathrm{mm}$ as a function of y. The cut corresponds to the y axis in Fig. 9.

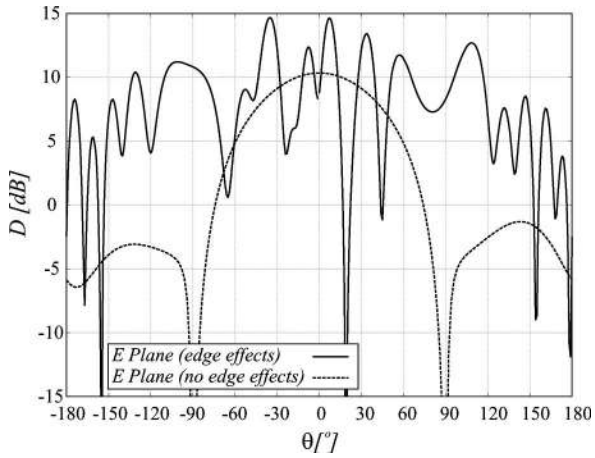

Fig. 12. Simulated co-polar radiation pattern of the array in the E-plane with no EBG. The dashed line corresponds to the simulation with and infinite substrate, while the solid curve includes the effects of the surface wave diffraction at the dielectric slab edges.

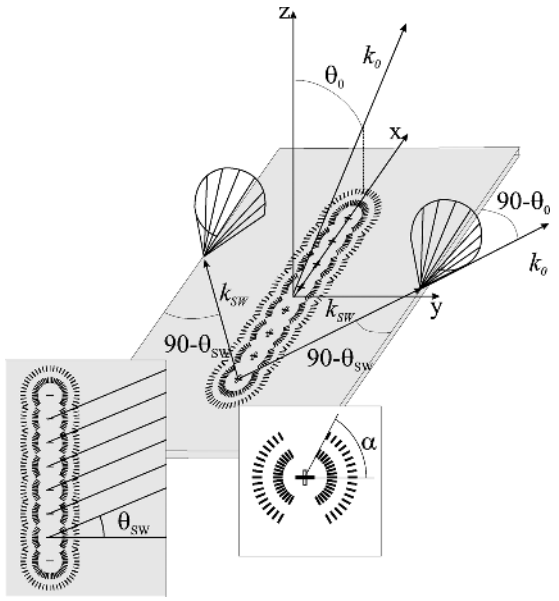

Fig. 11. Graphical view of the surface wave diffraction on the edge.

did not account for surface wave diffraction (infinite dielectric layer). The surface waves generated by a single antenna present a cylindrical spreading in all radial directions, and therefore the associated power is dispersed over a wide angular sector. In the present array configuration, the residual surface waves (not completely attenuated by the EBG) have a stronger impact on the radiation pattern and can be more easily identified. In fact, in the present array case the surface wave power is not spread over a large angular sector, but focused in certain *preferential* planes, because the surface waves form a unique coherent wave front in the direction dictated by the array phasing. For the broadside radiating case of Fig. 9, this direction is $\mathbf{i}_y$. In the inset of Fig. 11 one can see that the single surface waves launched by each of the elements of the array propagate along the dielectric slab surface forming an angle θ_{sw} with y. When the surface waves reach the dielectric edge (see Fig. 11), they are then radiated with maximum amplitude on a series of cones whose opening angles are defined imposing the continuity of the phase progression $k_{x0} = k_0 \sin\theta_0$.

The simulated E-plane radiation pattern of the array in absence of the EBG is shown in Fig. 12, when the elements are phased to obtain a broadside beam. The curves pertinent to prediction from CST (that include edge diffraction) and the ones pertinent to Ansoft Designer (that do not include edge diffraction) are compared. One can observe that due to edge diffraction effects the two patterns are significantly different. The difference is significantly bigger than in the cases shown in [7]. Although the use of absorbing material to cover the edges of the finite slab would allow the reduction/suppression of these edge diffraction effects on the radiation pattern, the antenna still would be characterized by a very low surface wave efficiency of 41%. This corresponds to a gain reduction of 4 dB, which in turn corresponds to an effective antenna surface less than half of the physical one. The behavior of the array in the presence of the EBGs will be discussed in Section V where the corresponding measured radiation patterns are shown and an increase of overall performances is observed.

From a design perspective, it is useful to relate the angle at which surface wave are launched, θ_{sw}, to the angle that defines the EBG sectors, α as in Fig. 4. When $\theta_{\mathrm{sw}} > \alpha$, the surface wave is not blocked by the EBG. In this situation the array efficiency will be reduced due to the fact that the surface wave launched is three times larger than the one that would encounter the complete two EBG rings with normal incidence. Another factor that must be taken into account is the dispersion of the TM_0 mode. Its propagation constant varies significantly within the investigated bandwidth: starting from a low value of $k_{\mathrm{sw}} = 1.2k_0$ at 10 GHz it arrives to $k_{\mathrm{sw}} = 1.49k_0$ at 12 GHz. This variation implies that, if one attempts to scan the array to a certain angle θ_0, at different frequencies, different values of the angle α should be retained in the design to guarantee that the surface waves are efficiently blocked. In particular, α must satisfy the condition $\alpha > \theta_{\mathrm{sw}}$, where θ_{sw} is given by the following relation: $k_{x0} = k_0 \sin\theta_0 = k_{\mathrm{sw}} \sin\theta_{\mathrm{sw}}$. It is straight forward to verify that for $\theta_0 = 50°$, at 10 GHz α should be larger than 40°

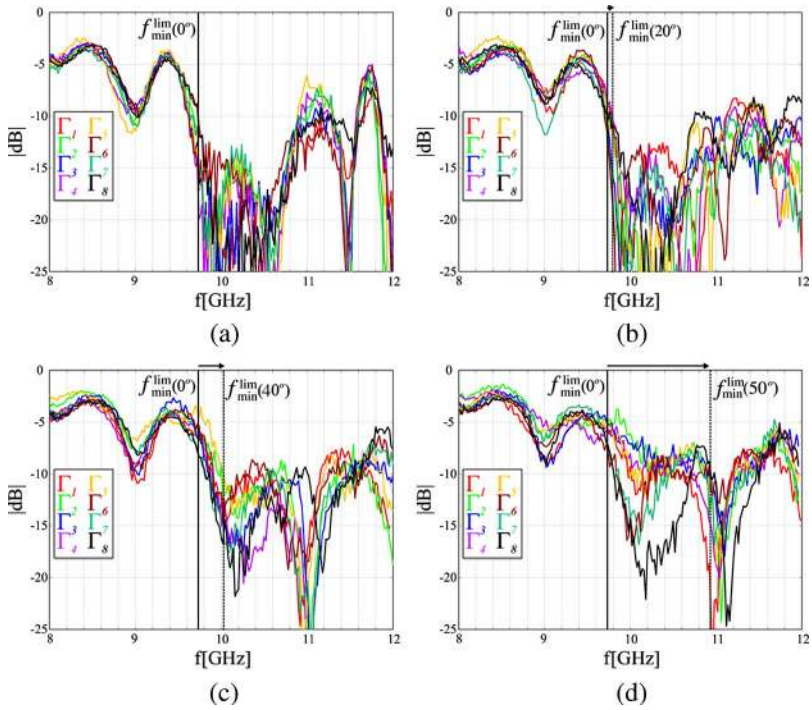

Fig. 13. Measured active reflection coefficients at four different phase shifting conditions associated to scanning toward $\theta = 0, 20^\circ, 40^\circ$, and 50° at 11 GHz.

to avoid the strong launching of surface waves, while at 12 GHz an EBG with only $\alpha > 31^\circ$ is needed. The absence of surface wave blockage, besides causing the loss of power via uncontrolled surface waves, also adversely effects the active matching properties of the array.

B. Active Reflection Coefficient

The measured active reflection coefficients of all the array elements are plotted in Fig. 13 as function of the frequency. These coefficients are derived as the ratio between the amplitude of the reflected and incident waves measured using directional couplers, directly before the coaxial to microstrip connections, see Fig. 8(b).

The curves in the different graphs correspond to four different phase shifting conditions, associated to scanning towards $\theta = 0^\circ, 20^\circ, 40^\circ$, and 50° at 11 GHz. Note that since the phase shift is not compensated for the deviation of the frequency from the nominal 11 GHz, the four graphs are only first approximations of the reflection coefficients at actual beam scanning situations. Despite this approximation, Fig. 13 shows that for low scanning angles, up to 20°, the relative BW over which the array can be operated with reflection coefficients below -10 dB is in the order of 20%. The periodical oscillations, visible over the entire BW and for all scanning angles, are associated to standing waves due to small mismatches between the antennas and the coaxial to microstrip connectors (this has been confirmed by numerical simulations). A significant bandwidth reduction is however observed for larger scanning angles. To understand the active reflection coefficient, as a function of the frequency and for different phase shifts, one should recall that a reduced $(\alpha \approx 40^\circ)$ EBG angular sector is used (see Fig. 4). For broadside radiation, the main surface wave direction $\theta_{\text{sw}} = 0$ is easily blocked by the EBGs and correspondingly the lower frequency limit for the -10 dB reflection coefficient is at $f_{\min}^{\lim} = 9.75$ GHz, see the dashed lines in Fig. 13. Also for phase shifts corresponding to $\theta_0 = 20^\circ$, the EBG is capable of blocking most of the surface waves launched by the arrays. However, a small degradation is expected due to the fact that a larger percentage of power is not blocked by the EBGs, with respect to the broadside case. This small degradation is observed in the reflection coefficient curves in the form of $f_{\min}^{\lim} = 9.8$ GHz. For phase shifts corresponding to $\theta_0 = 40^\circ$, the shift toward higher values of $f_{\min}^{\lim}$ is more evident. In the extreme case $\theta_0 = 50^\circ$ the EBG blockage of the surface waves is essentially lost and thus $f_{\min}^{\lim} = 10.9$ GHz.

V. Radiation Patterns

The radiation patterns of the array have been measured at the central frequency of 11 GHz.

A. H-Plane Cuts

The H plane will be considered first, with the co- and cross-polarized radiation patterns shown in Fig. 14, for the case of broadside radiation. The patterns are normalized to their maximum value and the comparison with the results predicted by CST simulations shows good agreement. The cross-polarized patterns are 30 dB below the co-polar radiation maximum. For scanning at $\theta_0 = 40^\circ$, the co- and cross-polarized H-patterns are shown in Fig. 15. Also the pattern simulated with Ansfot Designer is reported for comparison reasons. In this case, the maximum measured directivity is 1.4 dB lower than in the broadside case. Considering that the effective array area, when scanning to 40°, is reduced by a factor $\cos(40) = 0.766$, which corresponds to 1.15 dB, one can conclude that the surface wave diffraction has indeed a reduced impact on the H-plane pattern also for relatively large scanning angles. The beam is clean and the only noticeable aspect is that the cross polarization patterns is also

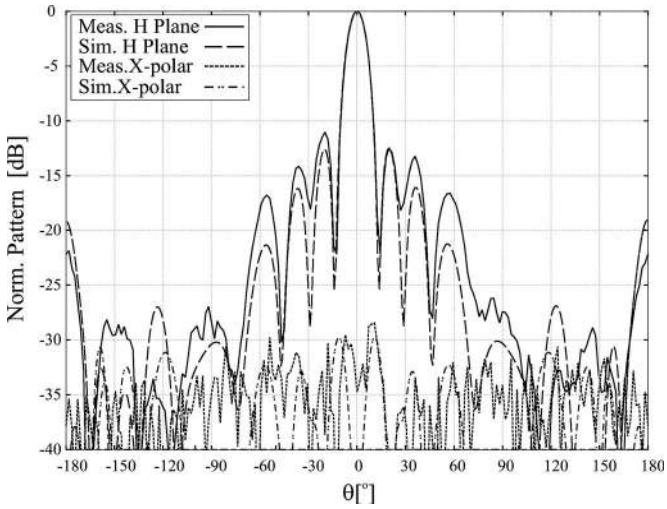

Fig. 14. Measured and calculated co-polar and cross-polar normalized radiation patterns at broadside in the H-plane at $f = 11$ GHz.

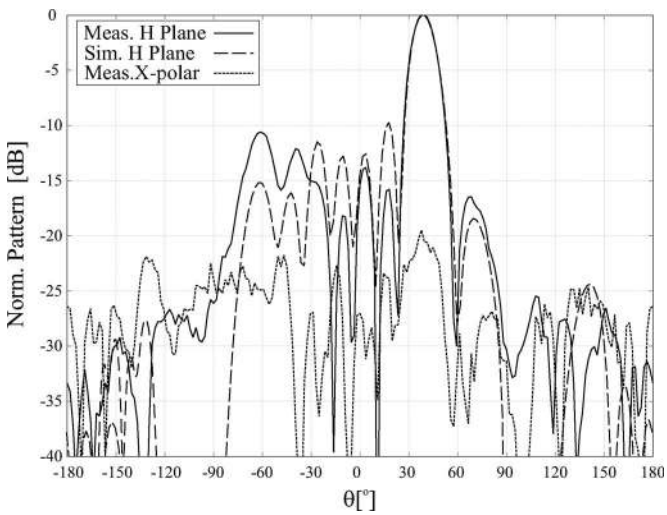

Fig. 15. Measured and calculated co-polar and cross-polar normalized radiation patterns at 40° scanning in the H-plane at $f = 11$ GHz. The maximum measured directivity when the array scans at $\theta_0 = 40°$ is 1.4 dB lower than in the broadside case.

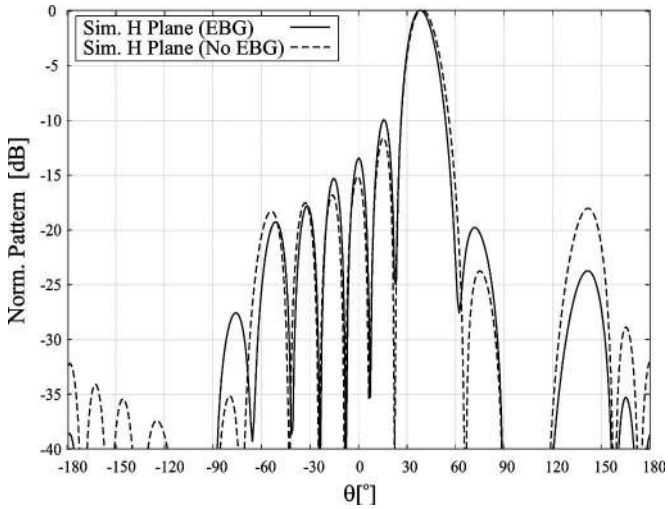

Fig. 16. Calculated co-polar normalized radiation patterns at 40° scanning in the H-plane at $f = 10$ GHz, for the array with and without EBGs.

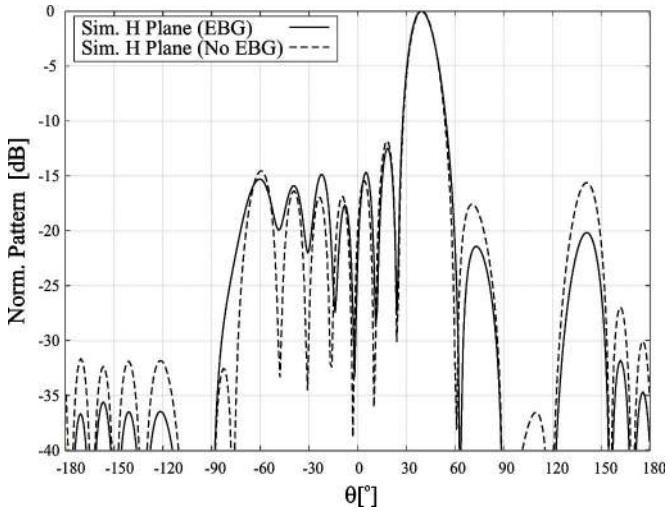

Fig. 17. Calculated co-polar normalized radiation patterns at 40° scanning in the H-plane at $f = 11.6$ GHz, for the array with and without EBGs.

maximum for $\theta_0 = 40°$. This seems to be due to surface wave diffraction contributions that for this scanning angle contribute directly to the cross-polarized pattern. This seems to be confirmed by the fact that similar cross polarized fields have been observed in the simulations of a smaller 4 elements array.

The array has been simulated with Ansoft Designer at lower and higher frequencies. Fig. 16 shows the H-plane for $\theta_0 = 40°$ at $f = 10$ GHz, while Fig. 17 shows the same pattern at $f = 11.6$ GHz. In order to show the effect of the EBG on this plane, the H patterns of the array without EBGs are also shown in the figures. The patterns have been normalized to their maximum value, even if the peak gains are significantly different for both arrays. It can be seen that side lobe levels are lager in case of EBGs for lower frequencies. This is associated to the fact that the sector blockage is more critical at lower frequencies (see Section IV-A). Therefore the residual surface wave propagating along the array is stronger and consequently its diffraction at the end-point is higher.

B. E-Plane Cut

The E plane co- and cross-polarized radiation patterns are shown in Fig. 18 for the case of broadside radiation. In this case, the patterns are not normalized and the values shown correspond to the measured and calculated directivities as a function of the angle. The feeding network implementation, with Wilkinson dividers, presented non-negligible losses and did not allow accurate gain measurements. However, since the dielectric slabs consist of very high quality ceramic based materials $(\tan(\delta) = 0.002)$, the ohmic and dielectric losses are negligible. Thus the directivities and the gains should essentially coincide for the antenna array under investigation if no power is lost into surface waves. It can be seen that simulations performed via CST and measurements are fairly similar with differences that are within calculation and measurement accuracy.

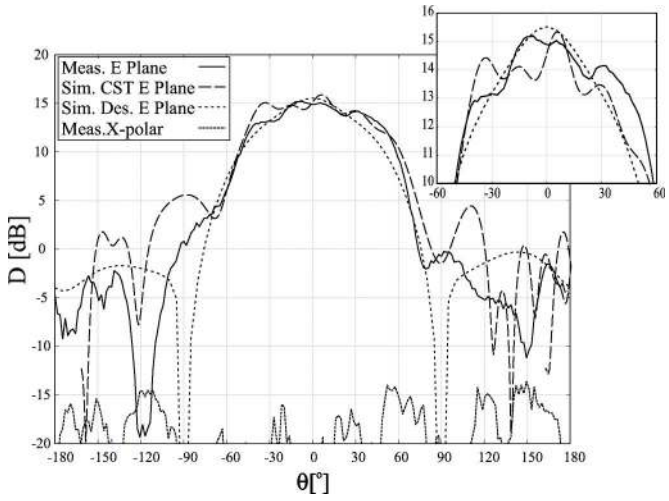

Fig. 18. Measured co-polar and cross-polar directivities in the E-plane at $f = 11$ GHz.

TABLE I
SIMULATED DIRECTIVIY AND GAIN

	f [GHz]	10	10.5	11	11.6
Array with EBGs	$D(0^o)$	17,8	16,8	15,7	14,3
	$G(0^o)$	15,7	16	15,6	13,6
	$D(20^o)$	17,9	16,7	15,4	14,7
	$G(20^o)$	15,2	16,1	14,8	14,1
	$D(40^o)$	17,2	16,2	15,9	14,9
	$G(40^o)$	13,3	15,6	14,8	14,2

	f [GHz]	10	10.5	11	11.6
Array without EBGs	$D(0^o)$	14,2	13,7	15	15,3
	$G(0^o)$	8,8	10,2	10,4	10,8
	$D(20^o)$	14,7	14,6	15,3	15,3
	$G(20^o)$	8,7	10,6	10,3	10,7
	$D(40^o)$	14,7	15,1	15,3	15,4
	$G(40^o)$	7,9	9,4	9,2	9,4

The actual values in both cases oscillate around the values predicted for an infinite substrate (Ansoft Designer simulations). This explicitly shows that the effect of the residual surface wave diffraction is still somehow present in the E-plane. The patterns were measured only at one frequency but it is apparent that the oscillations of the pattern around the value predicted by Designer are frequency dependent.

For the evaluation of the radiation pattern in the E-plane, two different criteria can be used: power radiated within the -3 dB angle of the main beam and shape of the radiation pattern.

In the first case, if one can accept the limited variations observed in the measured main beam pattern, then the overall power radiated within the -3 dB angle predicted by Ansoft Designer (no effect of surface waves diffraction by the edges) should be taken as a reference. Comparing this to the corresponding quantity including edge diffraction (measured pattern or CST simulation), then it can be concluded that no power is actually lost, on the contrary an overall improvement is obtained.

In the second case, in order to remove the edge diffraction effects and have a clean radiation pattern, it is necessary to dump the diffracted contribution. This can be done by introducing an absorbing material around the edges of the dielectric slab. The estimated surface wave efficiency of the array is in the order of 85%, which means that the remaining power is dumped into the absorbers. In this case, the actual directivity pattern is the one predicted by Ansoft Designer. The power lost (≈ 0.7 dB) is still not high considering that the gain of the antenna had already been increased by about 5 dB with respect to the same array without EBGs, see Fig. 12. As already explained in [7], this increase is partially due to the surface wave suppression and partially due to the larger effective area associated to the presence of the EBGs.

In Fig. 18, one can also observe the cross-polarized pattern which is 30 dB below the maximum co-polarized pattern. Simulation results of the cross-polarization fall outside the selected plot scale.

In order to show the frequency behavior, Table I shows the directivity (D) and gain (G) simulated with Ansoft Designer for the array with EBGs and without EBGs. The gain is systematically lower than the directivity and the difference is a measure of the efficiency of the array. This efficiency includes both matching and surface wave losses. The simulations are done for several frequencies and scanning angles. In case without EBGs, the gain is much lower than the directivity due to the low SW efficiency. From this numbers the array appears to be well behaved over the entire frequency and angular scanning range.

VI. CONCLUSION

Guidelines for the design of 1-D scanning arrays in printed technology for SAR applications have been provided. On one side, the use of dense dielectrics improves the front to back ratio and facilitates the integration of the antenna. On the other side, completely planar technology is used to suppress the surface wave edge effects and to improve the bandwidth thanks to the circular symmetry (PCS-EBG).

An array prototype has been designed manufactured and measured. The results demonstrate that PCS-EBG technology can be used to enhance the efficiency, bandwidth, directivity and polarization purity of very low cost and low profile one dimensional scanning arrays. The bandwidth over which a single layer and completely planar array can be scanned until 40°, without significant losses, is extended to about 15%.

ACKNOWLEDGMENT

The authors gratefully thank F. Nennie for performing measurements on the prototype. Gratitude is also expressed to the anonymous reviewers for accurate and useful suggestions.

REFERENCES

[1] L. L. Shafai, W. A. Chamma, M. Brakat, P. C. Strickland, and G. Seguin, "Dual-band dual-polarized perforated microstrip antennas for SAR applications," *IEEE Trans. Antennas Propag.*, vol. 48, no. 1, pp. 58–66, Jan. 2000.

[2] J. Granholm and K. Woelders, "Dual polarization stacked microstrip patch antenna array with very low cross polarization," *IEEE Trans. Antennas Propag.*, vol. 49, no. 10, pp. 1393–1402, Oc. 2001.
[3] R. B. Waterhouse, "Design and scan performances of large, probe-fed stacked microstrip patch arrays," *IEEE Trans. Antennas Propag.*, vol. 50, no. 6, pp. 893–895, Jun. 2002.
[4] Y. Fu and N. Yuan, "Elimination of scan blindness in phased array of microstrip patches using EBG materials," *IEEE Antennas Wireless Propag. Lett.*, vol. 3, pp. 63–65, 2004.
[5] F. Yang and Y. Rahmat-Samii, "Microstrip antennas integrated with EBG structures: a low mutual coupling design for array applications," *IEEE Trans. Antennas Propag.*, vol. 51, no. 10, pp. 2936–2946, Oct. 2003.
[6] Z. Iluz, R. Shavit, and R. Bauer, "Microstrip antenna phased array with electromagnetic bandgap substrate," *IEEE Trans. Antennas Propag.*, vol. 52, no. 6, pp. 1446–1453, Jun. 2004.
[7] N. Llombart, A. Neto, G. Gerini, and P. de Maagt, "Planar circularly symmetric EBG structures for reducing surface waves in printed antennas," *IEEE Trans. Antennas Propag.*, vol. 53, no. 10, pp. 3210–3218, Oct. 2005.
[8] A. Neto, N. Llombart, G. Gerini, and P. de Maagt, "On the optimal radiation bandwidth of printed slot antennas surrounded by EBGs," *IEEE Trans. Antennas Propag.*, vol. 54, no. 4, pp. 1074–1083, Apr. 2006.
[9] *"Ansoft Designer. Electromagnatically Charged EDA Software v1.1. Getting Started Guide,"* Ansoft Corporation, 2003.
[10] *"CST Microwave Studio, User Manual Version 5.0,"* CST GmbH, Darmstadt, Germany.

Nuria Llombart (S'06–M'07) received the Ingeniero de Telecomunicación degree and the Ph.D. degree from the Universidad Politécnica de Valencia, Spain, in 2002 and 2006, respectively.

She spent one year 2000 to 2001, at the Friedrich-Alexander University of Erlangen-Nuremberg, Germany, and worked at the Fraunhofer Institute for Integrated Circuits in Erlangen, Germany, from 2000 until 2002. Since 2002, she has been working as a Researcher at the Defence, Security and Safety Institute of the Netherlands Organization for Applied Scientific Research (TNO) in The Hague, The Netherlands. Her research interests include numerical and analytical methods for the analysis and design of printed antennas and EBG structures.

Dr. Llombart's Ph.D. was financed and hosted by the Defence, Security and Safety Institute of the Netherlands Organization for Applied Scientific Research (TNO) in The Hague, The Netherlands

Andrea Neto (M'00) received the Laurea degree (*summa cum laude*) in electronic engineering from the University of Florence, Florence, Italy, in 1994 and the Ph.D. degree in electromagnetics from the University of Siena, Siena, Italy, in 2000.

Part of his Ph.D. was developed at the European Space Agency Research and Technology Center, Noordwijk, The Netherlands, where he worked for over two years in the Antenna Section. From 2000 to 2001, he was a Postdoctoral Researcher at the California Institute of Technology, Pasadena, working for the S.W.A.T. Group of the Jet Propulsion Laboratory, Pasadena. Since 2002, has been a Senior Antenna Scientist at the Defence, Security and Safety Institute of the Netherlands Organization for Applied Scientific Research (TNO), The Hague, The Netherlands. His research interests are in the analysis and design of antennas, with emphasis on arrays, dielectric lens antennas, wideband antennas and EBG structures.

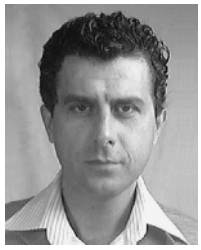

Giampiero Gerini (M'92) received the M.S. degree (*summa cum laude*) and Ph.D. degrees in electronic engineering from the University of Ancona, Ancona, Italy, in 1988 and 1992 respectively.

From 1994 to 1997, he was a Research Fellow at the European Space Research and Technology Centre (ESA-ESTEC), Nooordwijk, The Netherlands, where he joined the Radio Frequency System Division. Since 1997, he has been with the Netherlands Organization for Applied Scientific Research (TNO), The Hague, The Netherlands. At TNO Defence, Security and Safety, where he is currently Chief Senior Scientist of the Antenna Unit in the Transceivers and Real-time Signal Processing Department. His main research interests are phased array antennas, frequency selective surfaces and integrated front-ends.

Peter de Maagt (S'88–M'88–SM'02) was born in Pauluspolder, The Netherlands, in 1964. He received the M.Sc. and Ph.D. degrees from Eindhoven University of Technology, Eindhoven, The Netherlands, in 1988 and 1992, respectively, both in electrical engineering.

He is currently with the European Space Research and Technology Centre (ESTEC), European Space Agency, Noordwijk, The Netherlands. His research interests are in the area of millimeter and submillimeter-wave reflector and planar integrated antennas, quasi-optics, photonic bandgap antennas, and millimeter- and submillimeter-wave components.

Dr. de Maagt was a co-recipient of the H.A. Wheeler award of the IEEE Antennas and Propagation Society for the Best Applications Paper in 2001. He was granted a European Space Agency award for innovation in 2002.